Bispectral fluorescence imaging combined with texture analysis and linear discrimination for correlation with histopathologic extent of basal cell carcinoma

Marica B. Ericson
Jesper Uhre
Charlotta Strandeberg
Chalmers University of Technology–Göteborg University
School of Physics and Engineering Physics
SE-412 96 Göteborg, Sweden

Bo Stenquist
Olle Larkö
Ann-Marie Wennberg
Sahlgrenska University Hospital–Göteborg University
Department of Dermatology
SE-413 45 Göteborg, Sweden

Arne Rosén
Göteborg University–Chalmers University of Technology
School of Physics and Engineering Physics
SE-412 96 Göteborg, Sweden

Abstract. Fluorescence imaging has been shown to be a potential complement to visual inspection for demarcation of basal cell carcinoma (BCC), which is the most common type of skin cancer. Earlier studies have shown promising results when combining autofluorescence with protoporphyrin IX (Pp IX) fluorescence, induced by application of δ-5-aminolaevulinic acid (ALA). In this work, we have tried to further improve the ability of this technique to discriminate between areas of tumor and normal skin by implementing texture analysis and Fisher linear discrimination (FLD) on bispectral fluorescence data of BCCs located on the face. Classification maps of the lesions have been obtained from histopathologic mapping of the excised tumors. The contrast feature obtained from co-occurrence matrices was found to provide useful information, particularly for the ALA-induced Pp IX fluorescence data. Moreover, the neighborhood average features of both autofluorescence and Pp IX fluorescence were preferentially included in the analysis. The algorithm was trained by using a training set of images with good agreement with histopathology, which improved the discriminability of the validation set. In addition, cross validation of the training set showed good discriminability. Our results imply that FLD and texture analysis are preferential for correlation between bispectral fluorescence images and the histopathologic extension of the tumors. © 2005 Society of Photo-Optical Instrumentation Engineers. [DOI: 10.1117/1.1925650]

Keywords: autofluorescence; aminolaevulinic acid; basal cell carcinoma; Fisher linear discriminant; bispectral fluorescence imaging; texture analysis.

Paper 04053 received Apr. 5, 2004; revised manuscript received Oct. 15, 2004; accepted for publication Feb. 10, 2005; published online Jun. 16, 2005.

1 Introduction

Fluorescence imaging has been of increasing interest for its application in cancer detection in recent years.[1–6] The main advantage of the technique is that it is noninvasive and relatively fast, which is clearly favorable for clinical use. The occurrence of skin cancer is increasing worldwide, and it has been reported that the most common malignancy in the Caucasian population is basal cell carcinoma (BCC).[7] Early detection and delineation of the tumor border are often difficult, since the tumors may be irregular or invisible to the naked eye, leading to incomplete removal and high recurrence risks. Therefore, fast and effective tools for diagnosis of BCC are in great demand, and the fluorescence imaging technique has become an interesting complement to visual demarcation.[1–3]

By applying δ-5-aminolaevulinic acid (ALA) to the skin, the feedback control mechanism of the heme synthesis is bypassed, leading to accumulation of protoporphyrin IX (Pp IX).[8] Due to enzymatic alterations[9] and reduced penetration barrier of tumors,[10] the formation of endogenous Pp IX, after application of ALA, has been found to be higher in tumor compared to normal tissue.[8,11] Hence, ALA-induced Pp IX can serve as a fluorescence marker for tumors. The elevated red Pp IX fluorescence seems to correlate with the tumor extension of BCCs,[1–3] although there have been studies presenting a lack of fluorescence selectivity.[12]

Tissue fluorescence without the application of an external fluorophore is called autofluorescence.[13] Increased metabolism in the tumor region seems to be the key factor for causing decreased green fluorescence in the tumor region when excited in the UV region.[14] It has been shown advantageous to combine the ALA-induced fluorescence with the autofluorescence. For example, Svanberg et al. were able to visualize BCCs by taking the ratio between the Pp IX fluorescence and the autofluorescence signal.[15] By this procedure, enhanced contrast between tumor tissue and normal skin was obtained.

When developing new diagnostic tools, the real challenge is to test the ability of the techniques to demarcate tumors by comparing with the actual histopathologic extent of the lesions. In an earlier study from our group, the ALA-induced

Address all correspondence to M. B. Ericson, Department of Dermatology, Sahlgrenska University Hospital–Göteborg University, 413 45 Göteborg, Sweden. Tel: +46 (0)31 342 13 34; Fax: +46 (0)31 82 18 71; E-mail: marica.ericson@fy.chalmers.se

fluorescence of BCCs was compared with the histopathologic extent obtained from Mohs micrographic surgery.[1] More recently, we have extended the technique to include a multispectral imaging system assisted by image warping for alignment of the acquired images.[16,17] The results obtained were promising although further analysis and improvement are needed.

To our knowledge, the reports of fluorescence demarcation of BCC so far have been restricted to investigating only the basic intensity feature of the data. By performing texture analysis, additional data can be extracted from the images. This has been shown, for example, by Zhang et al. who performed a feasibility study of multispectral reflectance images for classification of skin lesions.[18] By calculating co-occurrence matrices,[19] second-order image statistics were obtained.

Since texture analysis in combination with bispectral images will increase the number of parameters, reduction of the dimensionality of data is needed. A classical technique for linear transformation of multidimensional data is the Fisher linear discriminant (FLD).[20] The principle of FLD is to find the linear combination of variables which maximizes the ratio of its between-group variance to its within-group variance, hence optimizing the discriminability.

In this work we have implemented texture analysis and FLD on image data from bispectral fluorescence imaging of aggressive infiltrating BCCs located in the face. The lesions were imaged before and after ALA application, in two different wavelength regions, recording both autofluorescence and Pp IX fluorescence. The tumors were excised with Mohs micrographic surgery to give a histopathologic map of each lesion. The images as well as the histopathologic maps were aligned by using image warping. The ability of the technique to discriminate between pixels corresponding to tumor and normal pixels has been evaluated by comparing receiver operation characteristics (ROC) curves. Both cross-validation and validation based on supervised training have been carried out.

2 Description of Fisher Linear Discriminant

The idea of FLD is to project the $D \times n$ dimensional data matrix X onto a vector, $\mathbf{a}$, so that the projected data, $\mathbf{y} = \mathbf{a}^T X$, are easier to classify. This is achieved by choosing the transformation vector $\mathbf{a}$ so that the ratio of the between-groups variance and the within-groups variance is maximized. The data matrix has n number of observations and D dimensions so that $X \in \mathbb{R}^{D \times n}$. Each observation $\mathbf{x}_j$ is a column of X and can be assigned to a certain group G_i. The mean value of each group expressed with the transformed data develops to

$$\mu_i = \frac{1}{n_i} \sum_{y_j \in G_i}^{y_j = \mathbf{a}^T \mathbf{x}_j} y_j = \frac{1}{n_i} \sum_{\mathbf{x}_j \in G_i} \mathbf{a}^T \mathbf{x}_j = \mathbf{a}^T \boldsymbol{\mu}_i, \quad (1)$$

where $\boldsymbol{\mu}_i$ is the mean vector of the untransformed data. In the case of two groups, the FLD is found by maximizing the ratio

$$J(\mathbf{a}) = \frac{|\mu_1 - \mu_2|^{2(1)}}{\sigma_1^2 + \sigma_2^2} = \frac{|\mathbf{a}^T(\boldsymbol{\mu}_1 - \boldsymbol{\mu}_2)|^2}{\sigma_1^2 + \sigma_2^2}, \quad (2)$$

Table 1 Filter combinations and spectral distribution for bispectral imaging.

	Autofluorescence	Pp IX fluorescence
Excitation	BG23, UG1 (365±5 nm)	BG23 [365±5 nm (95%), 405±3 nm (5%)]
Emission	BG23, GG420 (470±50 nm)	RG610 (610–700 nm)

where σ_i^2 is the variance of group G_i. For larger sets of data, it is suitable to write Eq. (2) in matrix form as

$$J(\mathbf{a}) = \frac{\mathbf{a}^T B \mathbf{a}}{\mathbf{a}^T W \mathbf{a}}. \quad (3)$$

The group scatter matrix, B, is defined as

$$B = (\boldsymbol{\mu}_1 - \boldsymbol{\mu}_2)(\boldsymbol{\mu}_1 - \boldsymbol{\mu}_2)^T, \quad (4)$$

and W is the total inner scatter matrix $W = \Sigma\, W_i$, where W_i is the inner scatter matrix for each group:

$$W_i = \sum_{\mathbf{x}_j \in G_i} (\mathbf{x}_j - \boldsymbol{\mu}_i)(\mathbf{x}_j - \boldsymbol{\mu}_i)^T. \quad (5)$$

Taking the derivative of J, Eq. (3), with respect to $\mathbf{a}$ and setting it to zero gives the generalized eigenvector problem $B\mathbf{a} = \lambda W\mathbf{a}(\mathbf{a}^T W\mathbf{a} \neq 0)$, with the solution

$$\mathbf{a} = W^{-1}(\boldsymbol{\mu}_1 - \boldsymbol{\mu}_2), \quad (6)$$

which is the resulting linear discriminant.

3 Methodology

3.1 Patients

Fifteen patients [six men, nine women, mean age 67 years (range 41–84)] with BCC on the face were included at the Department of Dermatology, Sahlgrenska University Hospital, Göteborg, Sweden. The study was approved by the local ethics committee and conducted in compliance with the protocol and according to Good Clinical Practice. All patients gave their informed consent before enrollment in the study. Three patients were excluded from the analysis. In one patient no tumor tissue was found during Mohs surgery. Additionally, two lesions located on the ear were excluded due to failure of image warping and problems in acquiring a complete histopathologic mapping.

3.2 Bispectral Fluorescence Imaging

The bispectral imaging set up consisted of two mercury lamps for fluorescence excitation and a thermoelectrically cooled charged coupled device (CCD) camera (Photometrics SenSys, Roper Scientific Inc., Tucson, AZ, USA). The two filter combinations used for imaging the autofluorescence and the Pp IX fluorescence are presented in Table 1. The filter combinations were chosen to match the absorption and emission peaks of the autofluorescence[14] and Pp IX fluorescence.[1] The total intensity of the excitation light was <0.5 mW/cm^2 and the ex-

posure time of the camera was 2 s for both recordings. The output raw data images were 512×512 pixels and 16-bit format, but were converted to 8-bit format after gray level thresholding.

The area to be investigated included the BCC lesion and approximately 2 cm of the surrounding normal skin. An ALA cream (Crawford Pharmaceuticals Ltd, England) consisting of 20% (w/w) ALA was applied for 3 h to obtain optimal Pp IX contrast between tumor and normal skin.[21] The lesion of interest was marked with four spots in ink used as landmarks for image analysis. A background Pp IX image was obtained before application of ALA. After the imaging procedure, the area was covered with an occlusive dressing for 48 h, to minimize the risk of undesired phototoxic reactions.

3.3 Histopathologic Map

All BCCs were excised by Mohs micrographic surgery without prior knowledge of the fluorescence results. The mean delay between the time of fluorescence investigation and surgical excision of tumor was 46 days±28 (mean±SD). Since BCCs are slow growing tumors, the changes in the tumors occurring during this time period can be neglected.[22] The excision site was inscribed with a black line in a reference image before surgery. The excised tissue blocks were frozen and re-embedded in paraffin. From these blocks, 4 μm sections were cut from the surface into the block at 3–4 levels. All microscopically verified tumor tissue was mapped to a separate chart for each section. By adding the tumor areas for each section a final map of the lateral extent of the tumor was obtained, without prior knowledge of the fluorescence images. The acquired histopathologic map was matched with the fluorescence images by using image warping, as will be described in the following. The precision of matching was estimated to be ±3 mm.

3.4 Image Warping

In order to match the different fluorescence images acquired at different times, image warping was applied. The applied algorithm was the affine transformation[23] described as

$$u = \alpha_{10}x + \alpha_{01}y + \alpha_{00},$$
$$v = \beta_{10}x + \beta_{01}y + \beta_{00}, \tag{7}$$

where x and y are the landmark coordinates of the input image, which are transformed to the position u, v in the output image. The parameters α_{ij} and β_{ij} describe the transformation.

For aligning the fluorescence images, four landmarks in each image were used. When aligning the histopathologic map with the macroscopic excision, up to ten landmarks were used, manually selected along the excision border. The algorithm was implemented in Matlab® (The MathWorks, Inc., Natick, MA, USA). The selected landmarks were inserted in two landmark matrices, Y and X, resulting in an overdetermined linear system $Y = XP$. The unknown parameter matrix P was determined by finding the least-square solution, giving the transformation parameters α_{ij} and β_{ij}. The desired transformation was thereafter carried out using Matlab® Image Processing Toolbox. A schematic picture of the image-processing procedure is presented in Fig. 1.
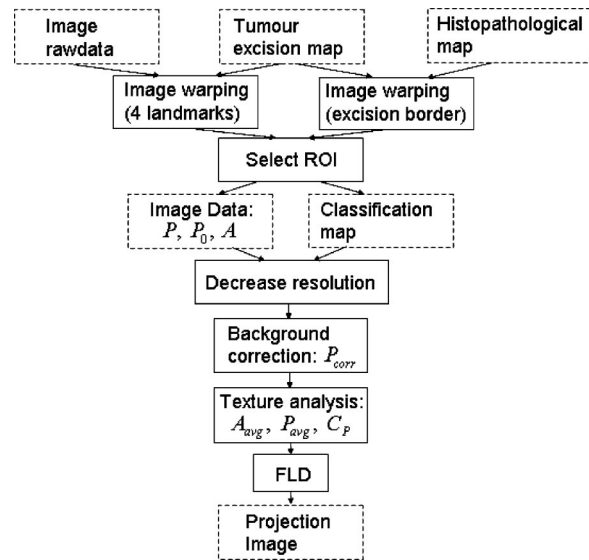

Fig. 1 Schematic drawing of image analysis procedure.

3.5 Image Preprocessing

To minimize computational time a region of interest (ROI) was selected. When choosing a ROI, care was taken to exclude disturbing edges, such as the border between ALA-treated skin and untreated skin. The pixel dimensions of a ROI varied between 75×107 and 227×232 depending on the lesion. The Pp IX images, P, were corrected by subtracting the background Pp IX images, P_0, giving the corrected Pp IX image, P_{corr}.

3.6 Texture Analysis

The average neighborhood features, A_{avg} and P_{avg}, were obtained by convolving the autofluorescence image, A, and the P_{corr} image with an averaging filter of size 10×10 pixels. The averaging works as a low-pass filter suppressing noise in the image.

Texture description by using co-occurrence matrices is based on the repeated gray-level configuration in an image window.[19] The matrix is constructed by calculating the relative frequencies $P_{\phi,d}(a,b)$, which describe how frequently pixel pairs with separation d in direction ϕ and gray levels (a,b), occur in a specified window centered around pixel (i,j). For each image pixel, the contrast, $C_{\phi,d}(i,j)$, can be calculated from the corresponding co-occurrence matrix as

$$C_{\phi,d}(i,j) = \sum_{a,b} |a-b|^2 P_{\phi,d}(a,b). \tag{8}$$

By constructing the co-occurrence matrices for various directions, ϕ, but fixed distance, d, the total contrast can be obtained by summing:

$$C_d(i,j) = \sum_{\phi} C_{\phi,d}(i,j). \tag{9}$$

The contrast parameter gives a measure for the variability of the fluorescence, where areas with high contrast signal have varying intensity.

Co-occurrence matrices were calculated for each pixel by a window of 21×21. The number of gray-scale levels were reduced from 256 to 51 to decrease computational time. The distance vector, d, was set to 3 pixels, and the angles were $0°$, $45°$, and $90°$. Subsequently the contrast image C was derived by calculating the contrast for all pixels.

3.7 Choice of Training Set

The fluorescence images were initially evaluated by calculating Z images, obtained as

$$Z = \frac{P - kP_0}{A}. \tag{10}$$

A similar procedure has been described earlier by Andersson-Engels et al.[2] The parameter k was introduced to account for intensity differences between P and P_0.

The Z images were compared with the histopathologic mapping and the degree of correlation was rated. The ratings revealed good correlation in four patients, and seven patients showed partial agreement. One patient showed deviating autofluorescence behavior, i.e., increased autofluorescence in the tumor region. Hence this patient was excluded from analysis. The fluorescence images with good correlation between Z image and histopathology were used as training set (labeled t1–t4) for the FLD algorithm, and the seven with partial agreement were used as validation set (labeled v1–v7).

3.8 Implementation of Fisher Linear Discriminant

The data matrix X was constructed by vectorization of the image data. For convenience the dimensions of X were shifted compared to earlier description of FLD so that $X \in \mathbb{R}^{n \times D}$. The ROI from each image was rescaled so that 10 000 pixels from each image set were incorporated in X. The solution of the Fisher function (6) was implemented according to a method described by Ripley.[24] The technique is based on singular value decomposition (SVD) of the data. First, SVD was carried out on the data matrix, giving $X = U_1 \Lambda_1 V_1^T$. The data were rescaled, $X_{rs} = XS$. Choosing

$$S = \sqrt{n} V_1 \Lambda_1^{-1} \tag{11}$$

simplifies the within-group covariance matrix for the rescaled variables so that it equals the identity matrix, i.e., $X_{rs}^T X_{rs} = nI$.

The elements of the group matrix, G, indicate which group each data point belongs to, $G_{ij} = \delta([i], j)$, where $[i]$ is the group of the data point i. By this definition, $G^T G$ is diagonal. The group means for the rescaled variables was calculated by $M = (G^T G)^{-1} G X_{rs}$. The diagonal matrix T was constructed by defining its elements as $T_{jj} = \sqrt{n/n_j}$, so that $T^T G^T G T = nI$. By performing a second SVD on

$$T^{-1} M = U \Lambda V^T, \tag{12}$$

one obtains

$$M = TU \Lambda V^T. \tag{13}$$

Hence, the group scatter matrix takes the form

$$\overset{(13)}{B} = (GM)^T GM = nV \Lambda^2 V^T, \tag{14}$$

and the inner scatter matrix becomes

$$\overset{(14)}{W} = X_{rs}^T X_{rs} - B = nV[I - \Lambda^2]V^T. \tag{15}$$

The Fisher function [Eq. (2)] can now be expressed as

$$J(\mathbf{a}) = \frac{\mathbf{a}^T B \mathbf{a}}{\mathbf{a}^T W \mathbf{a}} \overset{(14),(15)}{\underset{(\mathbf{b}=V^T\mathbf{a})}{=}} \frac{\mathbf{b}^T \Lambda^2 \mathbf{b}}{\mathbf{b}^T[I - \Lambda^2]\mathbf{b}} = \frac{\Sigma_i \lambda_i^2 b_i^2}{\Sigma_i (1 - \lambda_i^2) b_i^2}, \tag{16}$$

which will be maximized if only b_1 is nonzero. Since $\mathbf{a} = V\mathbf{b}$, the best choice of $\mathbf{a}$ will be in the direction of the first column of V, i.e., $\mathbf{v}_1$. So for the rescaled variables, $X_{rs}\mathbf{v}_1$ will maximize $J(\mathbf{a})$. Subsequently, the maximum of $J(\mathbf{a})$ is found for $XS\mathbf{v}_1$. The resulting linear discriminant will be

$$\mathbf{a}_{FLD} = S\mathbf{v}_1, \tag{17}$$

where S is obtained from the first SVD according to Eq. (11) and V is from the second SVD; see Eq. (12). By using other columns of V, more discriminants with decreasing order of discriminability can be obtained.

3.9 Validation

Cross validation (leave one out) was performed by using the training set. Thereafter the complete training set was applied to train the algorithm and validate it with respect to the validation set. The discriminability was evaluated by ROC. ROC curves are obtained by plotting the number of true positives (TP) against the number of false positives (FP). For a given discriminability the shape of the ROC curve will vary. The steeper the slope for low values of FPs, the better the discriminability of the method.

4 Results

In this paper we have used FLD for discrimination of tumor pixels and pixels corresponding to normal skin in bispectral fluorescence images of BCCs located in the face. Texture analysis has been implemented to increase the level of information extracted from the images. It was found that the best parameters to include in the algorithm were the neighborhood average of the autofluorescence, A_{avg}, and of the Pp IX fluorescence, P_{avg}, as well as the contrast feature of the background-corrected Pp IX image, C_P.

Figure 2 shows the scatter plots (a–c) of the in-going features of the training set and the projection on first and second Fisher vectors, $a_{FLD,1}$ and $a_{FLD,2}$, obtained from the training set. The histograms for A_{avg}, P_{avg}, and the projection on $a_{FLD,1}$, are also included in Figs. 2(d)–2(f). As can be seen from the scatter plots, the separation between the two different data groups is improved after projection on the FLD. This is especially true for the projection on the first discriminant. As expected, the tumor pixels tend to be located towards lower A_{avg} values [Fig. 2(d)] and higher P_{avg} [Fig. 2(e)]. In the histogram for the projected data, Fig. 2(f), the separation between the tumor and normal groups is improved.

Figure 3 shows the resulting FLDs during cross validation. As expected, the P_{avg} images have a positive correlation with
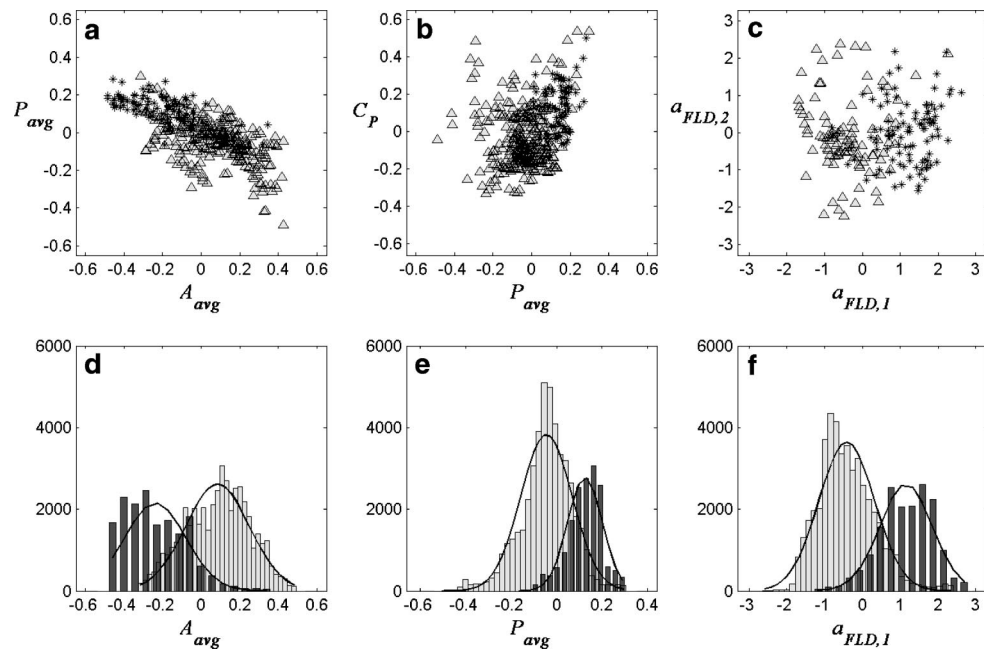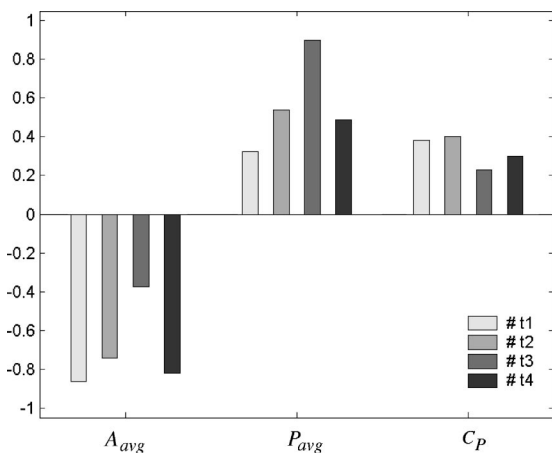
Fig. 2 (a)–(c) Scatterplots of data from the training set. P_{avg} and A_{avg} are the neighborhood averages of Pp IX fluorescence and autofluorescence, respectively. C_P is the Pp IX fluorescence contrast. $a_{FLD,1}$ and $a_{FLD,2}$ are the first and second linear discriminants. Pixels corresponding to normal skin are denoted by $\triangle$, and tumor pixels are denoted by $\ast$. Histograms for the data projected on A_{avg}, P_{avg}, and $a_{FLD,1}$ are shown in (d)–(f). Black bars belong to tumor class and gray bars represent the normal class.

tumor, whereas the correlation with A_{avg} images are negative. In addition, the contrast image, C_P, shows positive correlation. The ROC curves for the cross validation are shown in Fig. 4. As can be seen, the discriminability is particularly good for t2, and t3, reaching a high degree of TP and low values of FP. The deviation from the line of chance (LoC) was large for all cases.

As a second evaluation, the algorithm was trained by using the complete training set (t1–t4) and validated using the validation set (v1–v7). The overall result including the complete validation set is shown in Fig. 5. Included in the figure are the ROC curves for the basic features P and A. In addition, the Z feature, calculated as the ratio between P and A, is presented. As shown in Fig. 5, the ROC curves for P are actually below LoC. The Z feature shows some discriminability up to 20% of TP, which thereafter drops off. The A curve is the only curve of the simple features that shows some discriminability in the whole range. By performing FLD transformation in combination with texture analysis, the ROC curve is improved for the validation set.

Figure 6 shows photographs of two morpheiform BCCs, (a) t3 included in the training set and (b) v5 from the validation set. The fluorescence, texture and projection images for each lesion are presented in Figs. 7 and 8, respectively. As shown, there is an elevated Pp IX fluorescence (a) and de-

Fig. 3 Resulting linear discriminant, a_{FLD}, when performing cross validation of training set. A_{avg} and P_{avg} are the neighborhood averages of autofluorescence and Pp IX fluorescence respectively. C_P is the texture contrast of Pp IX fluorescence.
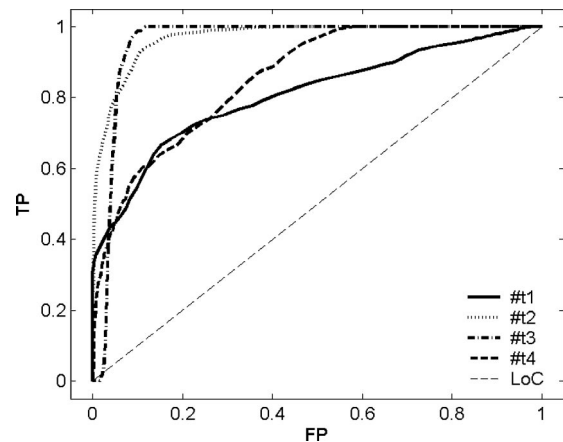
Fig. 4 Cross-validation ROC analysis, i.e., true positives (TP) against false positives (FP). The different image series are labeled t1–t4. Included is also the line of chance (LoC).
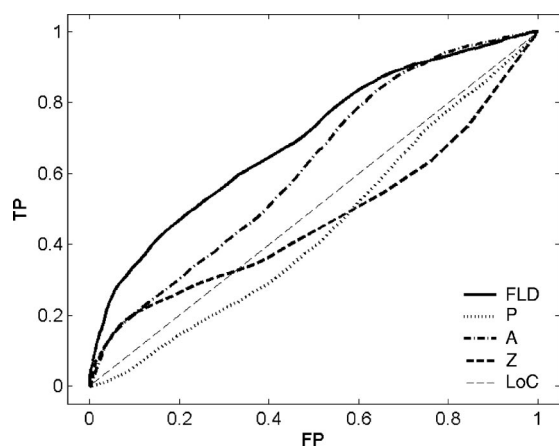
Fig. 5 ROC analysis of validation set, i.e., true positives (TP) against false positives (FP). The different lines represent different methods. Linear discrimination combined with texture analysis (FLD), Pp IX image only (P), autofluorescence only (A), and Z analysis (Z). Included is also the line of chance (LoC).

creased autofluorescence (b) in the tumor area. In the neighborhood average images (c,d), this behavior is more pronounced suppressing noise. However, in Fig. 8(c), there is an area outside the tumor which shows rather high Pp IX fluorescence. Interestingly, this area is not detected in the contrast image (e), implying that the fluorescence texture is homogeneous in this area. In the tumor, however, the fluorescence seems to be highly varying, which generally gives a strong signal in contrast image. In the resulting projection images (f), the agreement with the tumor border is shown.

5 Discussion

The demand for effective tools for diagnosis and demarcation of skin cancer is increasing, particularly for BCC which is the most common skin malignancy.[7] Fluorescence imaging using ALA-induced Pp IX as fluorescent marker, has shown a potential use for demarcation and delineating these types of tumors.[1–3] However, there are studies reporting on lack of selectivity of the Pp IX fluorescence.[12] It has proved to be preferential to combine the ALA-induced fluorescence with the autofluorescence.[15] By taking the ratio between the two different fluorescence signals, increased contrast has been obtained. Still, the question remains of how to demarcate between tumor tissue and normal skin.

In order to investigate the correlation between bispectral fluorescence images and the histopathologic extent of the tumor, some sort of matching technique is needed to be able to align the fluorescence data with the histology map. This can be obtained by performing image warping.[23] We have earlier presented a comparison between Z images, i.e., the ratio between Pp IX fluorescence and autofluorescence, and the histologic extent of BCCs.[17] In the present study we have investigated the possibility of using FLD in combination with texture analysis for improving and evaluating the discriminability of the technique. A training set of four cases with good agreement in the earlier study was implemented, and seven image series with partial agreement were used as the validation set. Both cross validation and evaluation using the validation set were carried out.

It was shown that the discriminability based on the ROC curves from the cross validation of the training set was good. In addition, the training of the implemented algorithm was found to significantly improve the discriminability of the validation set compared to the simple features. Interestingly, the autofluorescence alone was found to be the best basic feature to discriminate the pixels from the ROC analysis. Surprisingly, the P feature displayed a lack of discriminability. This shows that the Pp IX fluorescence alone is insufficient for tumor demarcation of some lesions. Despite this, the Pp IX fluorescence provides useful information when performing texture analysis, since the contrast feature increases the discriminability significantly.

In texture analysis, there is a huge variety of parameters which can be calculated; however, depending on the task, only a few of these will contain useful information. In this study we have tested parameters calculated from co-occurrence matrices[19] extracted from the different fluorescence images, in addition to neighborhood averaging. It was found that the contrast parameter and the neighborhood average contained useful data to discriminate between tumor and normal pixels. Hence, only these parameters were implemented in the discrimination algorithm.

It is important to try to understand the physical meanings of the actual texture parameters in order to eliminate the risk of implementing unrealistic parameters. For this purpose, the neighborhood average is possibly correlated with the fact that pixels classified as tumor are most likely to be surrounded by other tumor pixels. Sporadic fluorescence changes will be suppressed. The contrast parameter, on the other hand, gives a measure for the variability of the fluorescence in a certain area. Areas with varying intensity information will give a high contrast signal, whereas areas with homogeneous fluorescence are extinguished. This is of great importance in the case of ALA-induced fluorescence. It seems that the ALA-induced fluorescence is rather inhomogeneous in the tumor area, giving a high contrast signal. Moreover, artifacts due to uneven ALA distribution, causing elevated Pp IX levels without correspondence to tumor, will be suppressed since these areas show a different pattern compared to tumor areas. It was found that only the contrast parameter for the Pp IX fluorescence contained useful information. Hence, only the Pp IX contrast feature was included in the discriminant analysis.

When implementing FLD analysis, the choice of training set is of great importance. In this study we used image data whose fluorescence ratio earlier showed good agreement with the histopathologic map, as the training set. By doing so, we forced the algorithm to find a linear discriminant representative for these data. Still, the derived discriminant was able to improve the discriminability of the validation set, which showed only partial agreement using the fluorescence ratio alone. It is possible that even better discrimination can be obtained by being able to subdivide the lesions into different groups, using different discriminants. For example, we have observed a lesion with increased autofluorescence in the tumor area which was excluded here because of its deviant behavior. This type of analysis requires a much larger corpus of patient material, and is therefore subject to future work.

As shown by this study, the contrast parameter obtained from co-occurrence matrices of the Pp IX images provided useful information for discrimination between tumor and nor-
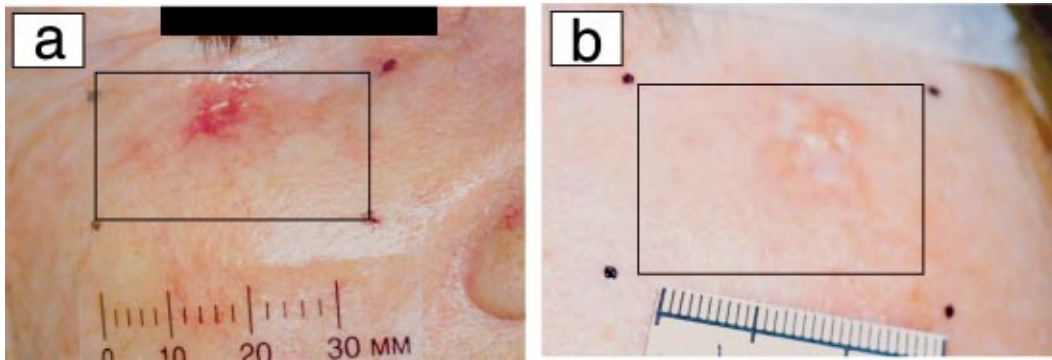
Fig. 6 Photography of two lesions. Morpheiform BCC located (a) under right eye, included in training set, t3 and (b) at forehead, included in validation set, v5. The black rectangle indicates the ROI, for which fluorescence data have been obtained (see Figs. 7 and 8).
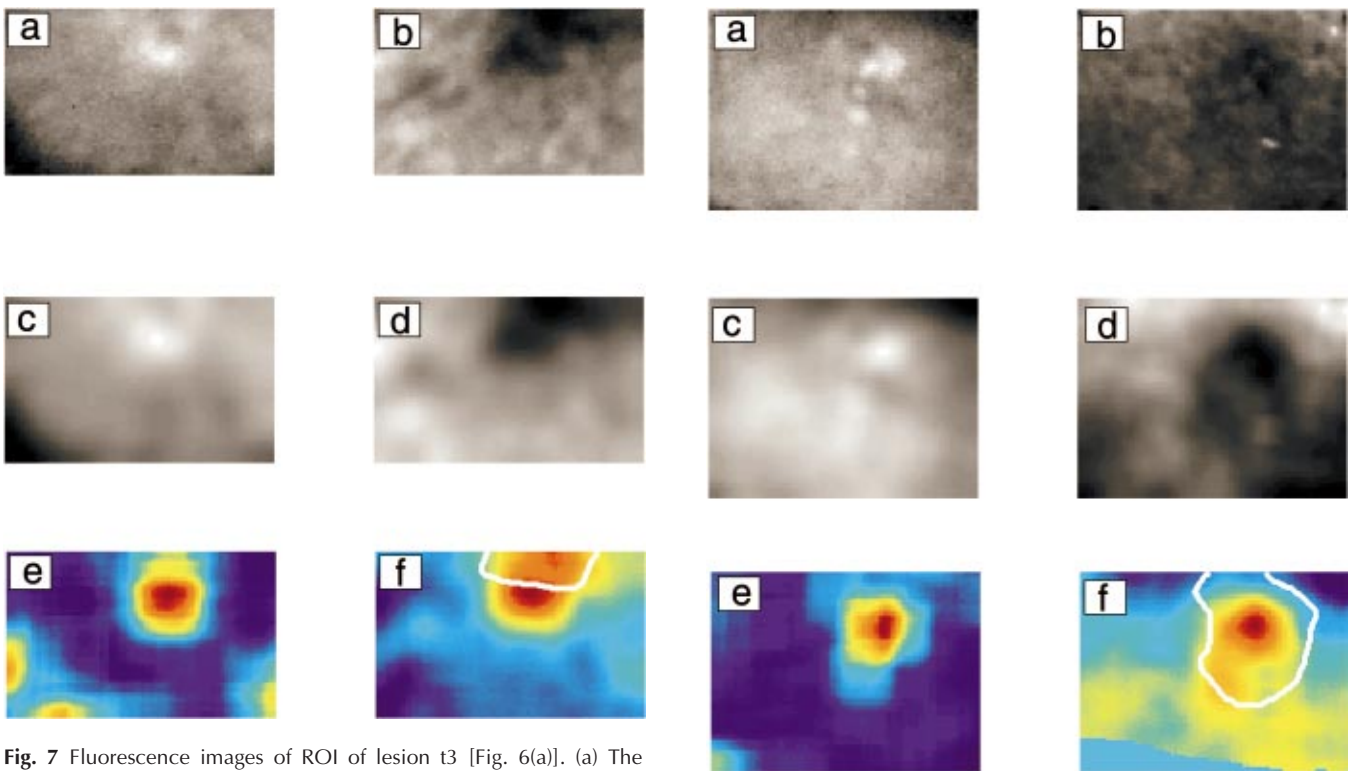
Fig. 7 Fluorescence images of ROI of lesion t3 [Fig. 6(a)]. (a) The corrected Pp IX fluorescence, P_{corr}, (b) the autofluorescence image, A, (c) the average image of P_{corr}, P_{avg}; (d) shows the average image of A, A_{avg}, (e) is the calculated contrast image from P_{corr}, C_P, and (f) shows the final projection image, a_{FLD}. Delay between fluorescence investigation and surgery was 33 days.

Fig. 8 Fluorescence images of ROI of lesion v5 [Fig. 6(b)]. (a) The corrected Pp IX fluorescence, P_{corr}, (b) the autofluorescence image, A, (c) the average image of P_{corr}, P_{avg}; (d) shows the average image of A, A_{avg}, (e) is the calculated contrast image from P_{corr}, C_P, and (f) shows the final projection image, a_{FLD}. Delay between fluorescence investigation and surgery was 53 days.

mal areas. A major drawback associated with this parameter, however, is that of edge effects. Since the contrast is high in areas with a high degree of fluorescence variation, edges will give a strong signal. For example, the border between the ALA-treated area and the non-ALA-treated surrounding skin may cause a false signal. This can be observed in Fig. 7(e), in the lower left-hand corner. For this reason, it is of great importance to be able to obtain a ROI without edges in order to be able to use this texture feature.

Another problem noted in this study is the disturbing effect of hair in the autofluorescence images. It is likely that the keratin in hair causes the disturbance. This problem occurs if the lesion is located on the scalp or in the close vicinity of the hairline. It appears that shaving is not sufficient to eliminate the unwanted fluorescence completely. Since many tumors have this location, it is desirable to find techniques minimizing this problem.

In conclusion, we have investigated the possibility of improving the ability to discriminate tumor areas from normal skin in fluorescence images of BCCs, by implementing texture analysis in combination with FLD. Classification maps of the lesions have been obtained from histopathologic mapping of the excised tumors. Even though the study was based on a limited data set, it was found that the contrast parameter obtained from co-occurrence matrices of the ALA-induced Pp IX fluorescence, together with the neighborhood average of autofluorescence and Pp IX fluorescence, provides useful information for the discrimination task. By training the algorithm, using a training set of images with good agreement with histopathology, the discriminability of images with only partial agreement was improved. These results imply that when applying bispectral fluorescence imaging for demarcation of skin lesions, FLD and texture analysis are preferential for obtaining correlation between images and the histopathologic extent of the tumors. Nonetheless, further studies are needed to make the technique robust as a diagnostic tool.

Acknowledgments

References

1. A. M. Wennberg, F. Gudmundson, B. Stenquist, A. Ternesten, L. Mölne, A. Rosén, and O. Larkö, "In vivo detection of basal cell carcinoma using imaging spectroscopy," *Acta Derm Venereol* **79**(1), 54–61 (1999).
2. S. Andersson-Engels, G. Canti, R. Cubeddu, C. Eker, C. af Klinteberg, A. Pifferi, K. Svanberg, S. Svanberg, P. Taroni, G. Valentini, and I. Wang, "Preliminary evaluation of two fluorescence imaging methods for the detection and the delineation of basal cell carcinomas of the skin," *Lasers Surg. Med.* **26**(1), 76–82 (2000).
3. G. Ackermann, C. Abels, S. Karrer, W. Baumler, M. Landthaler, and R. M. Szeimies, "Fluorescence-assisted biopsy of basal cell carcinomas," *Hautarzt* **51**(12), 920–924 (2000).
4. V. Nadeau, K. Hamdan, J. Hewett, W. Sibbett, I. Tait, A. Cuschieri, and M. Padgett, "Endoscopic fluorescence imaging and point spectroscopy system for the detection of gastro-intestinal cancers," *J. Mod. Opt.* **49**(5–6), 731–741 (2002).
5. B. Mayinger, M. Jordan, P. Horner, C. Gerlach, S. Muehldorfer, B. R. Bittorf, K. E. Matzel, W. Hohenberger, E. G. Hahn, and K. Guenther, "Endoscopic light-induced autofluorescence spectroscopy for the diagnosis of colorectal cancer and adenoma," *J. Photochem. Photobiol., B* **70**(1), 13–20 (2003).
6. W. Zheng, M. Olivo, and K. C. Soo, "The use of digitized endoscopic imaging of 5-ALA-induced PPIX fluorescence to detect and diagnose oral premalignant and malignant lesions in vivo," *Int. J. Cancer* **110**(2), 295–300 (2004).
7. H. Tran, K. Chen, and S. Shumack, "Epidemiology and aetiology of basal cell carcinoma," *Br. J. Dermatol.* **149**(s66), 50–52 (2003).
8. J. C. Kennedy and R. H. Pottier, "Endogenous protoporphyrin IX, a clinically useful photosensitizer for photodynamic therapy," *J. Photochem. Photobiol., B* **14**(4), 275–292 (1992).
9. S. L. Gibson, D. J. Cupriks, J. J. Havens, M. L. Nguyen, and R. Hilf, "A regulatory role for porphobilinogen deaminase (PBGD) in δ-aminolaevulinic acid (δ-ALA)-induced photosensitization?," *Br. J. Cancer* **77**(2), 235–243 (1998).
10. J. Moan, L. W. Ma, and V. Iani, "On the pharmacokinetics of topically applied 5-aminolevulinic acid and two of its esters," *Int. J. Cancer* **92**(1), 139–143 (2001).
11. C. Abels, P. Heil, M. Dellian, G. E. Kuhnle, R. Baumgartner, and A. E. Goetz, "In vivo kinetics and spectra of 5-aminolaevulinic acid-induced fluorescence in an amelanotic melanoma of the hamster," *Br. J. Cancer* **70**(5), 826–833 (1994).
12. A. Martin, W. D. Tope, J. M. Grevelink, J. C. Starr, J. L. Fewkes, T. J. Flotte, T. F. Deutsch, and R. R. Anderson, "Lack of selectivity of protoporphyrin IX fluorescence for basal cell carcinoma after topical application of 5-aminolevulinic acid: implications for photodynamic treatment," *Arch. Dermatol. Res.* **287**(7), 665–674 (1995).
13. H. S. Zeng, C. Macaulay, B. Palcic, and D. I. McLean, "A computerized autofluorescence and diffuse reflectance spectroanalyzer system for in vivo skin studies," *Phys. Med. Biol.* **38**(2), 231–240 (1993).
14. R. Richards-Kortum and E. Sevick-Muraca, "Quantitative optical spectroscopy for tissue diagnosis," *Annu. Rev. Phys. Chem.* **47**, 555–606 (1996).
15. K. Svanberg, I. Wang, S. Colleen, I. Idvall, C. Ingvar, R. Rydell, D. Jocham, H. Diddens, S. Bown, G. Gregory, S. Montan, S. Andersson-Engels, and S. Svanberg, "Clinical multi-colour fluorescence imaging of malignant tumours—initial experience," *Acta Radiol.* **39**(1), 2–9 (1998).
16. M. B. Ericson, C. Berndtsson, B. Stenquist, A.-M. Wennberg, O. Larkö, and A. Rosén, "Multispectral fluorescence imaging of basal cell carcinoma assisted by image warping," *Proc. SPIE* **5141**, 114–121 (2003).
17. M. B. Ericson, C. Berndtsson, B. Stenquist, L. Mölne, A.-M. Wennberg, O. Larkö, and A. Rosén, "Fluorescence demarcation of basal cell carcinoma controlled by histopathological mapping," *Proc. SPIE* **5370**, 1411–1418 (2004).
18. J. Zhang, C. I. Chang, S. J. Miller, and K. A. Kang, "A feasibility study of multispectral image analysis of skin tumors," *Biomed. Instrum. Technol.* **34**(4), 275–282 (2000).
19. R. M. Haralick, K. Shanmuga, and I. Dinstein, "Textural features for image classification," *IEEE Trans. Syst. Man Cybern.* **SMC-3**(6), 610–621 (1973).
20. R. O. Duda, P. E. Hart, and D. G. Stork, *Pattern Classification*, 2nd ed., Wiley, New York (2001).
21. M. B. Ericson, C. Sandberg, F. Gudmundson, A. Rosén, O. Larkö, and A. M. Wennberg, "Fluorescence contrast and threshold limit: implications for photodynamic diagnosis of basal cell carcinoma," *J. Photochem. Photobiol., B* **69**(2), 121–127 (2003).
22. P. M. Gordon, N. H. Cox, W. D. Paterson, and C. M. Lawrence, "Basal cell carcinoma: are early appointments justifiable?," *Br. J. Dermatol.* **142**(3), 446–448 (2000).
23. C. A. Glasbey and K. V. Mardia, "A review of image warping methods," *J. Appl. Stat.* **25**, 155–171 (1998).
24. B. D. Ripely, *Pattern Recognition and Neural Networks*, Cambridge University Press, Cambridge, U.K. (1996).